Protein Backbone Dynamics and ^{15}N Chemical Shift Anisotropy from Quantitative Measurement of Relaxation Interference Effects

Nico Tjandra, Attila Szabo, and Ad Bax*

Contribution from the Laboratory of Chemical Physics, National Institutes of Diabetes and Digestive and Kidney Diseases, National Institutes of Health, Bethesda, Maryland 20892-0520

Received February 16, 1996[⊗]

Abstract: Cross-correlation between ^{15}N−^{1}H dipolar interactions and ^{15}N chemical shift anisotropy (CSA) gives rise to different relaxation rates of the doublet components of ^{15}N−{^{1}H} peptide backbone amides. A simple scheme for quantitative measurement of this effect is described which yields information on the magnitude of the CSA from the relative intensities of ^{1}H−^{15}N correlations obtained with two slightly different pulse schemes. The method is applied to a sample of uniformly ^{15}N-enriched ubiquitin and measurements conducted at two field strengths (8.5 and 14 T) yield identical results. The degree of relaxation interference correlates with the isotropic ^{15}N chemical shift and results indicate that the sum of the most shielded principal components of the CSA tensor is nearly invariant to structural differences in the polypeptide backbone. The relaxation interference is directly proportional to the generalized order parameter, $\boldsymbol{S}^2$, of the peptide backbone amides, and this relation can be utilized to obtain approximate values for these order parameters.

There is a renewed interest in understanding the relation between protein structure and ^{13}C and ^{15}N chemical shifts.[1−3] Indeed, recent *ab initio* calculations show considerable promise for providing an accurate correlation between chemical shift and the structure of the peptide backbone. In proteins, the results of calculations could only be compared with the value of the isotropic chemical shift, as accurate values for the individual chemical shift anisotropy (CSA) tensor elements in proteins are not easily measured. Here we demonstrate that a measure for the magnitude of the CSA of individual peptide backbone ^{15}N nuclei can be obtained from quantitative measurement of interference effects between the CSA and dipolar relaxation mechanisms. The magnitude of the interference effect is expected to be directly proportional to the generalized order parameter, $\boldsymbol{S}^2$,[4,5] and this correlation is confirmed experimentally. Inversely, the simple relaxation interference measurement can be used to obtain the relative $\boldsymbol{S}^2$ values of the backbone amides.

Relaxation of peptide backbone ^{15}N nuclei in proteins is dominated by CSA and by the dipolar interaction between ^{15}N and its directly attached proton. Based on solid-state NMR studies of model compounds containing peptide bonds, the ^{15}N CSA tensor is nearly axially symmetric and its unique axis makes a relatively small angle of *ca.* 20−24° with the N−H bond vector.[6−9] As a result, for a ^{15}N nucleus attached to a proton in the $|\beta\rangle$ spin state the sum of the dipolar and CSA tensors is much smaller than for ^{15}N nuclei attached to a ^{1}H in the $|\alpha\rangle$ spin state, and the two types of ^{15}N nuclei relax at very different rates. This differential relaxation is commonly referred to as a cross-correlation or relaxation interference effect[10−15] and a simple treatment of this effect, directly applicable to the case of peptide ^{15}N−^{1}H amide pairs, has been presented by Goldman.[13] Although cross correlation forms the basis of several elegant heteronuclear magnetization transfer experiments,[16,17] more often it is considered a nuisance as it can alter the outcome of relaxation measurements if no precautions are taken to eliminate the effect.[18−20] Here we demonstrate that the effect can be used advantageously to obtain information on the ^{15}N CSA tensor and on the internal dynamics of the peptide backbone. The method is demonstrated for human ubiquitin, a small globular protein of 76 residues which is well-characterized by both X-ray crystallography[21] and numerous NMR studies.[22−27]

[⊗] Abstract published in *Advance ACS Abstracts,* July 1, 1996.

(1) de Dios, A. C.; Pearson, J. G.; Oldfield, E. *Science* **1993**, *260*, 1491−1496.
(2) Pearson, J. G.; Oldfield, E.; Lee, F. S.; Warshel, A. *J. Am. Chem. Soc.* **1993**, *115*, 6851−6862.
(3) Oldfield, E. *J. Biomol. NMR* **1995**, *5*, 217−225.
(4) Lipari, G.; Szabo. A. *J. Am. Chem. Soc.* **1982**, *104*, 4546−4558, 4559−4570.
(5) Elbayed, K.; Canet, D. *Mol. Phys.* **1989**, *68*, 1033−1046.
(6) Oas, T. G.; Hartzell, C. J.; Dahlquist, F. W.; Drobny, G. P. *J. Am. Chem. Soc.* **1987**, *109*, 5962−5966.
(7) Hiyama, Y.; Niu, C.-H.; Silverton, J. V.; Bavoso, A.; Torchia, D. A. *J. Am. Chem. Soc.* **1988**, *110*, 2378−2383.
(8) Lumsden, M. D.; Wasylishen, R. E.; Eichele, K.; Schindler, M.; Penner, G. H.; Power, W. P.; Curtis, R. D. *J. Am. Chem. Soc.* **1994**, *116*, 1403−1413.
(9) Shoji, A.; Ozaki, T.; Fujito, T.; Deguchi, K.; Ando, S.; Ando, I. *Macromolecules* **1989**, *22*, 2860−2863.
(10) McConnell, H. M. *J. Chem. Phys.* **1956**, *25*, 709−711.
(11) Mackor, E. L.; MacLean, C. *Prog. Nucl. Magn. Reson. Spectrosc.* **1967**, *3*, 129−157.
(12) Gueron, M.; Leroy, J. L.; Griffey, R. H. *J. Am. Chem. Soc.* **1983**, *105*, 7262−7266.
(13) Goldman, M. *J. Magn. Reson.* **1984**, *60*, 437−452.
(14) Wimperis, S.; Bodenhausen, G. *Mol. Phys.* **1989**, *66*, 897−919.
(15) Werbelow, L. G. *Encyclopedia of Nuclear Magnetic Resonance*; Grant, D. M., Harris, R. K., Editors-in-Chief; Wiley: London; Vol. 6, pp 4072−4078.
(16) Dalvit, C. *J. Magn. Reson.* **1992**, *97*, 645−650.
(17) Tolman, J. R.; Prestegard, J. H. *J. Magn. Reson. Ser. B* **1995**, *106*, 97−100.
(18) Boyd, J.; Hommel, U.; Campbell, I. D. *Chem. Phys. Lett.* **1990**, *175*, 477−482.
(19) Palmer, A. G., III; Skelton, N. J.; Chazin, W. J.; Wright, P. E.; Rance, M. *Mol. Phys.* **1992**, *75*, 699−711.
(20) Kay, L. E.; Nicholson, L. K.; Delaglio, F.; Bax, A.; Torchia, D. A. *J. Magn. Reson.* **1992**, *97*, 359−375.
(21) Vijay-Kumar, S.; Bugg, C. E.; Cook, W. J. *J. Mol. Biol.* **1987**, *194*, 531−544.
(22) Di Stefano, D. L.; Wand, A. J. *Biochemistry* **1987**, *26*, 7272−7281.
(23) Weber, P. L.; Brown, S. C.; Mueller, L. *Biochemistry* **1987**, *26*, 7282−7290.
(24) Schneider, D. M.; Dellwo, M.; Wand, A. J. *Biochemistry* **1992**, *31*, 3645−3652.
(25) Wang, A. C.; Grzesiek, S.; Tschudin, R.; Lodi, P. J.; Bax, A. *J. Biomol. NMR* **1995**, *5*, 376−382.
(26) Wang, A. C.; Bax, A. *J. Am. Chem. Soc.* **1996**, *118*, 2483−2494.

S0002-7863(96)00510-0

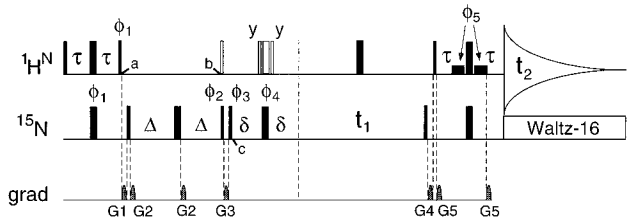

Figure 1. Pulse scheme for quantitative measurement of cross correlation. In the reference experiment (scheme B), the open ^{1}H 90° and composite ($90_y-220_x-90_y$) 180° pulses are not applied, whereas they are applied in scheme (A), where all resonances are the result of cross correlation effects during the period 2Δ. Narrow and wide pulses correspond to flip angles of 90° and 180°, respectively. The two low power pulses immediately preceding and following the last non-selective ^{1}H 180° pulse have a width of 1 ms each and correspond to flip angles of 90°. With the carrier positioned on the H_2O resonance, they are part of the WATERGATE water suppression scheme.[39] The radio-frequency phase of all pulses is assumed *x*, unless indicated. Delay durations: $\tau \approx 2.4$ ms; $\delta = 2.67$ ms, $T_2/8 < \Delta < T_2/2$. Phase cycling: $\phi_1 = y,-y$; $\phi_2 = x,x,-x,-x$; $\phi_4 = 4(x),4(y),4(-x),4(-y)$; $\phi_5 = -x$; Receiver = $x,-2(-x),x,-x,2(x),-x$. Quadrature detection in the t_1 dimension is accomplished by incrementing ϕ_3 in the States-TPPI manner. All gradients are sine-bell shaped, with an amplitude of 25 G/cm at their center. Durations: G1,2,3,4,5 = 2.75, 2, 1, 1.5, and 0.4 ms.

Experimental Section

All NMR experiments were carried out at 27 °C on a sample of commercially obtained (U-^{15}N)-ubiquitin (VLI Research, Southeastern, PA), 1.4 mM, pH 4.7, 10 mM NaCl. Experiments were carried out on Bruker AMX-360 and AMX-600 NMR spectrometers operating at ^{1}H resonance frequencies of 360 and 600 MHz, respectively. Both spectrometers were equipped with pulsed field gradient ^{1}H/^{15}N probeheads, optimized for ^{1}H detection.

Data matrices acquired at both 360 and 600 MHz consisted of 128*-(t_1) × 768*(t_2) data points, with acquisition times of 64 (t_1) and 83 ms (t_2). A total of 32 scans per complex t_1 increment was collected in experiment B (Figure 1) at both 360 and 600 MHz, whereas 384 and 128 scans were accumulated in experiment A (Figure 1) at 360 and 600 MHz, respectively. All experiments were performed with the ^{1}H carrier positioned on the H_2O resonance and the ^{15}N carrier at 116.5 ppm. Durations for the dephasing delay, 2Δ, were 46.7, 68, and 132 ms at 600 MHz and 132 ms at 360 MHz.

All data sets were processed using 45° shifted sine-bell apodization and zero filling in both dimensions to yield a digital resolution of 2.3, 3.9 Hz (F_1) and 2.7, 4.5 Hz (F_2) for 360 and 600 MHz data respectively. Data were processed using nmrPipe[28] and analyzed with the program PIPP.[29] Resonance intensities were obtained from peak heights using three-data-point interpolation,[29] and resonance assignments are taken from Wang et al.[25]

Results and Discussion

Assuming an axially symmetric ^{15}N chemical shift tensor with an angle θ between the orientation of its unique axis and the N−H bond vector, the ^{15}N transverse relaxation rates for the two doublet components of an isolated ^{15}N−^{1}H spin pair are given by[5,13−15]

$$R_2 = \lambda \pm \eta \tag{1a}$$

where the + sign applies to the upfield ^{15}N doublet component ($^1J_{NH} < 0$) and λ and η are given by

$$\lambda = d[4J^{dd}(0) + 4\alpha^2 J^{cc}(0) + 3J^{dd}(\omega_N) + 3\alpha^2 J^{cc}(\omega_N) + J^{dd}(\omega_N - \omega_H) + 3J^{dd}(\omega_H) + 6J^{dd}(\omega_N + \omega_H)] \tag{1b}$$

$$\eta = 2\alpha d\{4J^{cd}(0) + 3J^{cd}(\omega_N)\} \tag{1c}$$

where $d = \gamma_H^2\gamma_N^2h^2/(80\pi^2r_{HN}^6)$, $\alpha = -4\pi/3B_o(\sigma_{||} - \sigma_\perp)r_{HN}^3/(h\gamma_H)$, and r_{NH} is the ^{15}N−^{1}H internuclear distance, assumed to be 1.02 Å. $J^{dd}(\omega)$, $J^{cc}(\omega)$, and $J^{cd}(\omega)$ are the spectral densities for dipolar autocorrelation, CSA autocorrelation, and dipolar-CSA cross correlation, respectively. For an axially symmetric CSA tensor, these spectral densities are given by

$$J^{pq}(\omega) = \int_0^\infty \langle P_2(\mu_p(0)\cdot\mu_q(t)\rangle \cos(\omega t)\, dt \tag{2}$$

where $\mu_p(t)$ is the unit vector describing the orientation of the axially symmetric interaction *p* at time *t*, and $P_2(x) = (3x^2 - 1)/2$. Assuming isotropic rotational diffusion of a rigid body, one has

$$J^{dd}(\omega) = J^{cc}(\omega) = J^{cd}(\omega)/P_2(\cos\theta) \tag{3}$$

where θ is the angle between the unique axes of the CSA and dipolar tensors, i.e., $\theta = \cos^{-1}(\mu_d(t)\cdot\mu_c(t))$. Although eq 3 is no longer rigorous in the presence of internal motion, results of calculations shown in the Appendix indicate it remains a very good approximation provided θ is small. Therefore, the superscripts in the spectral density function may be dropped and eq 1c is then rewritten as

$$\eta = 2\alpha d\{4J(0) + 3J(\omega_N)\}P_2(\cos\theta) \tag{4}$$

For the case of isotropic rotational diffusion and additional rapid internal motions, occurring on a time scale τ_e and described, in the model-free approach of Lipari and Szabo,[4] by a generalized order parameter $\boldsymbol{S}^2$, the spectral density function is defined as

$$J(\omega) = \boldsymbol{S}^2\tau_c/(1 + \omega^2\tau_c^2) + (1 - \boldsymbol{S}^2)\tau/(1 + \omega^2\tau^2) \tag{5}$$

with $\tau^{-1} = \tau_c^{-1} + \tau_e^{-1}$. The time constant τ_c is the rotational correlation time, assuming isotropic diffusion. However, rotational diffusion of ubiquitin is slightly anisotropic, and to a good approximation is described by an axially symmetric diffusion tensor, **D**, with $D_{||}/D_\perp = 1.17$.[27] In this case, calculation of the cross-correlation term becomes considerably more complex,[30,31] unless $\theta = 0°$. For $\theta = 0°$, one may simply use eq 1 in combination with the spectral density function applicable for axially symmetric rotational diffusion with internal motion:[32,33]

$$J(\omega) = \boldsymbol{S}^2\sum_k A_k\tau_k/(1 + \omega^2\tau_k^2) + (1 - \boldsymbol{S}^2)\tau/(1 + \omega^2\tau^2) \tag{6}$$

with $k = 1, 2, 3$ and $A_1 = 0.75 \sin^4\beta$, $A_2 = 3\sin^2\beta\cos^2\beta$, $A_3 = (1.5\cos^2\beta - 0.5)^2$, where β is the angle between the N−H bond vector and the unique axis of the rotational diffusion tensor; $\tau_1 = (4D_{||} + 2D_\perp)^{-1}$, $\tau_2 = (D_{||} + 5D_\perp)^{-1}$, $\tau_3 = (6D_\perp)^{-1}$, and $\tau^{-1} = \tau_e^{-1} + (2D_{||} + 4D_\perp)^{-1}$, where $D_{||}$ and $D_\perp$ are the rotational diffusion constants parallel and perpendicular to the unique axis of the diffusion tensor. For peptide ^{15}N nuclei θ is small (20−24°), and use of eqs 1 and 6 provides a reasonable approximation.

(27) Tjandra, N.; Feller, S. E.; Pastor, R. W.; Bax, A. *J. Am. Chem. Soc.* **1995**, *117*, 12562−12566.
(28) Delaglio, F.; Grzesiek, S.; Vuister, G. W.; Zhu, G.; Pfeifer, J.; Bax, A. *J. Biomol. NMR* **1995**, *6*, 277−293.
(29) Garrett, D. S.; Powers, R.; Gronenborn, A. M.; Clore, G. M. *J. Magn. Reson.* **1991**, *94*, 214−220.
(30) Chung, J.; Oldfield, E.; Thevand, A.; Werbelow, L. *J. Magn. Reson.* **1992**, *100*, 69−81.
(31) Szabo, A. *J. Chem. Phys.* **1984**, *81*, 150−167.
(32) Woessner, D. E. *J. Chem. Phys.* **1962**, *3*, 647−654.
(33) Barbato, G.; Ikura, M.; Kay, L. E.; Pastor, R. W.; Bax, A. *Biochemistry* **1992**, *31*, 5269−5278.

Measurement of Cross Correlation. Figure 1 shows the pulse scheme used for measuring the cross correlation effect quantitatively. The pulse scheme is essentially an HSQC ^{1}H−^{15}N correlation experiment,[34] with a relaxation period 2Δ inserted before the ^{15}N evolution period. The experiment is performed twice, once with applying the shaded ^{1}H 90° and composite ^{1}H 180° pulses, and once without applying these pulses. In the following these experiments will be referred to as A and B, respectively.

In both versions of the pulse scheme, ^{1}H magnetization (represented by S) is transferred to ^{15}N (represented by I) at time point *a* in Figure 1, and antiphase transverse ^{15}N magnetization, described by the operator product $2I_yS_z$, is generated by the first 90° ^{15}N pulse. The two ^{15}N doublet components are described by $I_yS_z \pm I_y/2$. The downfield doublet component, $I_yS_z - I_y/2$, relaxes at a rate $\lambda - \eta$, whereas the upfield component relaxes at $\lambda + \eta$ (*cf.* eq 1). Thus, after the dephasing delay 2Δ (time point *b* in Figure 1), the transverse magnetization is given by

$$\sigma_b = (I_yS_z - I_y/2)\exp[-2\Delta(\lambda - \eta)] + (I_yS_z + I_y/2) \times \exp[-2\Delta(\lambda + \eta)] = I_yS_z(\epsilon^+ + \epsilon^-) + I_y(\epsilon^+ - \epsilon^-)/2 \quad (7)$$

where $\epsilon^{\pm} = \exp[-2\Delta(\lambda \pm \eta)]$. At time point *b* the ^{15}N magnetization is returned to the *z* axis. In scheme A, the antiphase fraction of the ^{15}N *z* magnetization, $I_zS_z(\epsilon^+ + \epsilon^-)$, is destroyed by the sequential application of a 90° ^{1}H pulse and pulsed field gradient G3. The in-phase component, $I_z(\epsilon^+ - \epsilon^-)/2$, is converted to antiphase magnetization during the subsequent delay, 2δ, prior to t_1 evolution and transfer of ^{15}N magnetization to protons by the final reverse INEPT part of the pulse scheme. In scheme B, the 90° ^{1}H pulse is not applied and the I_zS_z ^{15}N magnetization is converted back into antiphase transverse ^{15}N magnetization at time point *c*. This $-I_yS_z(\epsilon^+ + \epsilon^-)$ term remains antiphase at the end of the delay 2δ, as the composite ^{1}H pulse is not applied in scheme B. After the t_1 evolution period, the ^{15}N magnetization is returned to observable proton magnetization, in a manner identical to that of scheme A. In the absence of the composite ^{1}H 180° pulse, the in-phase ^{15}N magnetization, $I_y(\epsilon^+ - \epsilon^-)/2$, remains in phase at the end of the t_1 evolution period and therefore does not contribute to the signal detected in scheme B. Thus, the ratio of the signal intensities obtained with schemes A and B equals

$$I_A/I_B = (\epsilon^- - \epsilon^+)/(\epsilon^- + \epsilon^+) = \tanh(2\Delta\eta) \quad (8)$$

Note that the losses caused by relaxation are essentially identical in schemes A and B. The faster relaxation of the I_zS_z term between time points *b* and *c* in scheme A, relative to the decay of I_z in scheme B, produces negligible relaxation loss because the duration of this delay (2 ms) is about two orders of magnitude shorter than the inverse of the difference in relaxation rates of I_zS_z and I_z. In addition to the very small relaxation loss between time points *b* and *c* in scheme B, there is also a loss of signal which occurs in scheme A and not in B, caused by the imperfection of the composite 180° ^{1}H pulse. As a test, adding a composite pulse between time points *b* and *c* in scheme B is found to change the average intensity of the ^{15}N−^{1}H correlations by a factor of −0.986, indicating that 99.3% of the protons are inverted by the composite pulse and the imperfection in this pulse therefore may be safely ignored. The I_A/I_B ratio divided by the uncertainty in this ratio caused by thermal noise is highest when $2\Delta \approx \lambda^{-1}$, i.e., when the duration of 2Δ is approximately equal to T_2. Thus, the random uncertainty in the derived CSA values is minimal when $2\Delta \approx T_2$. Note that in both schemes A and B the applicable value of T_2 is the average of the T_2 for in-phase and antiphase ^{15}N magnetization, which, on average, is about a third shorter than the in-phase T_2 measured in regular relaxation experiments.[35,36]

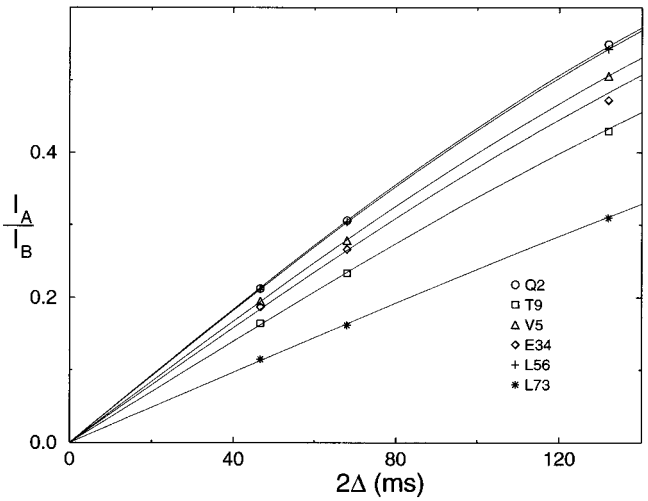

Figure 2. Ratio of intensities, I_A/I_B, obtained with schemes A and B of Figure 1, as a function of 2Δ, at 600-MHz ^{1}H frequency, for six different residues in ubiquitin. The drawn lines correspond to eq 8.

Figure 2 shows the I_A/I_B ratio as a function of 2Δ. As can be seen from this figure, the ratio agrees very well with the theoretical dependence of eq 8. This means that even for a dephasing time as long as T_2, there is no significant second-order effect on the I_A/I_B ratio. However, if durations of 2Δ longer than T_2 are used, such effects can become noticeable. For example, there is a cross-correlation effect between the ^{15}N−^{1}H^N dipolar interaction and the approximately 8 times smaller intraresidue ^{15}N−^{1}H$^\alpha$ dipolar interaction. In particular for φ backbone angles near −120°, where the two dipolar interactions are nearly collinear, such dipole−dipole cross correlation can give rise to a slight decrease of the measured I_A/I_B ratio.

As can be seen from eqs 4 and 8, the I_A/I_B ratio is a function of $\boldsymbol{S}^2(\sigma_{||} - \sigma_\perp)P_2(\cos\theta)$ and the effects of a variation in $\sigma_{||} - \sigma_\perp$ cannot be separated from a change in θ or $\boldsymbol{S}^2$. We refer to $\boldsymbol{S}^2(\sigma_{||} - \sigma_\perp)P_2(\cos\theta)$ as the reduced CSA, or CSA^{red}. $\boldsymbol{S}^2$ values for human ubiquitin have been derived previously from ^{15}N relaxation time measurements,[27] and based on solid-state NMR measurements on model compounds, θ is generally believed to fall between 20 and 24°,[6−9] which puts $P_2(\cos\theta)$ in the 0.825−0.75 range.

Figure 3 shows excellent agreement between CSA^{red} values measured at 600-MHz ^{1}H frequency for two different durations of 2Δ. A very small systematic decrease of *ca.* 1.1% in CSA^{red} observed for the longer duration of 2Δ is presumably caused by cross correlation between ^{15}N−^{1}H^N and ^{15}N−^{1}H$^\alpha$ dipolar interactions, mentioned above. The measurement was also repeated at 360-MHz ^{1}H frequency and again shows very good agreement with the data measured at 600 MHz (Figure 3B).

Figure 4 shows the values of CSA^{red} as a function of residue number. As expected the highly mobile C-terminal tail yields much smaller values for CSA^{red} than the remainder of the protein. After dividing CSA^{red} by the previously derived $\boldsymbol{S}^2$ value, the values become more homogeneous, with an average value of 140 ± 9 ppm (Figure 4B). Assuming a θ value of 20°, this yields an average value for $\sigma_{||} - \sigma_\perp$ of −170 ppm. This is slightly larger than the value of 160 ppm commonly

(34) Bodenhausen, G.; Ruben, D. J. *Chem. Phys. Lett.* **1980**, *69*, 185−189.

(35) Bax, A.; Ikura, M.; Kay, L. E.; Torchia, D. A.; Tschudin, R. *J. Magn. Reson.* **1990**, *86*, 304−318.

(36) Peng, J. W.; Thanabal, V.; Wagner, G. *J. Magn. Reson.* **1991**, *95*, 421−427.

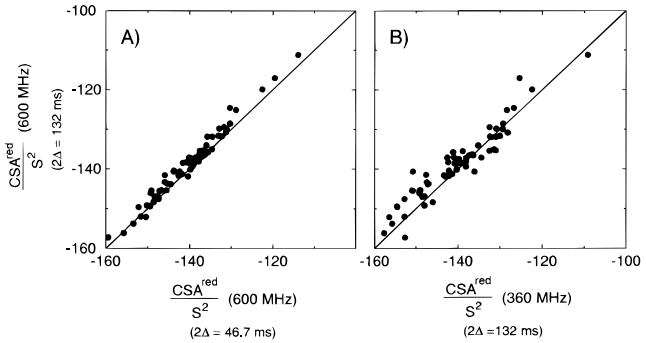

Figure 3. Comparison of CSA^{red} values measured from (A) data acquired at 600 MHz and 2Δ durations of 46.7 and 132 ms and (B) data acquired at 600 and 360 MHz, both for $2\Delta = 132$ ms.

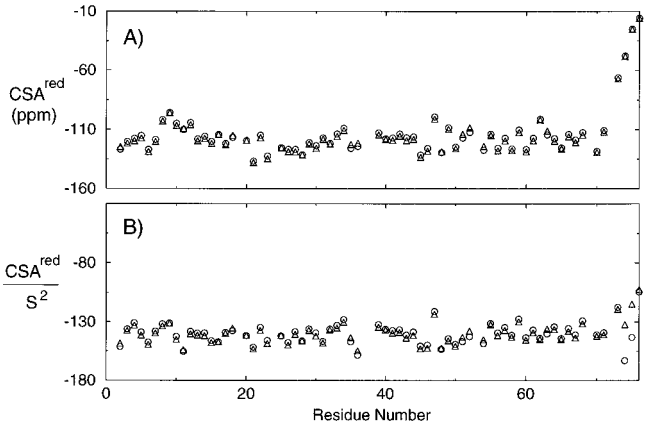

Figure 4. Values of (A) CSA^{red} and (B) $CSA^{red}/\boldsymbol{S}^2$ as a function of residue number in human ubiquitin. The CSA^{red} values have been calculated from data acquired at 600 MHz and $2\Delta = 46.7$ ms, assuming isotropic (○) and axially symmetric (Δ) rotational diffusion.

used for the magnitude of the CSA in ^{15}N relaxation studies. However, this latter value was based on the width of powder patterns observed in solid-state NMR spectra of polycrystalline peptides. As a result of rapid internal motions the width of these powder patterns is reduced by a factor $\boldsymbol{S}$ relative to the true value of the CSA.[7] The magnitude of the CSA observed in the present study therefore is in good agreement with previous solid-state NMR results.

Correlation between CSA and Isotropic Shift. The isotropic ^{15}N shift, δ, equals minus one-third of the trace of the chemical shift tensor: $\delta = -(\sigma_{11} + \sigma_{22} + \sigma_{33})/3$. The least shielded component, σ_{11}, is the one oriented in the peptide plane and nearly orthogonal to the C−N bond. The σ_{22} and σ_{33} components are most shielded and are of comparable magnitude in peptide bonds. For $\theta = 0°$, the magnitude of the cross-correlation effect is determined by $\sigma_{11} - (\sigma_{22} + \sigma_{33})/2$. Although this relation is only valid when $\theta = 0°$, the assumption of an axially symmetric tensor with $\sigma_{\|} - \sigma_{\perp} = \sigma_{11} - (\sigma_{22} + \sigma_{33})/2$ yields nearly the same magnitude for the cross-correlation term, provided $\theta < 25°$.

If the σ_{11}, σ_{22}, and σ_{33} values of the ^{15}N shielding tensors in ubiquitin are normally distributed, with standard deviations Δ_1, Δ_2, and Δ_3, respectively, the standard deviation for the isotropic shift is expected to be $^1/_3(\Delta_1^2 + \Delta_2^2 + \Delta_3^2)^{1/2}$, provided variations in σ_{11}, σ_{22}, and σ_{33} are uncorrelated. A decrease in σ_{22} or σ_{33} (*i.e.*, deshielding) gives rise to a smaller chemical shift anisotropy and a smaller value of the cross-correlation term, in addition to a downfield change of the isotropic shift. In contrast, a decrease in σ_{11} will *increase* the chemical shift anisotropy, but also give rise to a downfield change of the isotropic shift.

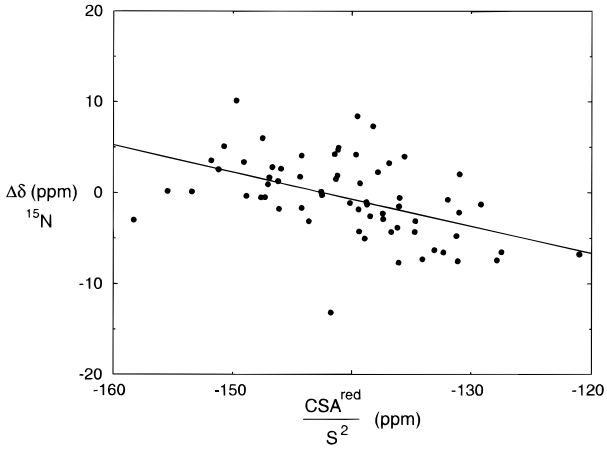

Figure 5. Correlation between $CSA^{red}/\boldsymbol{S}^2$ and the deviation, $\Delta\delta$, of the isotropic shift from the random coil value[38] for the backbone amide ^{15}N nuclei in human ubiquitin. CSA^{red} values are calculated from data recorded at 600 MHz, using the average of the values obtained for $2\Delta = 46.7$ and $2\Delta = 68$ ms and the axially symmetric diffusion parameters. Residues Leu^{73}-Gly^{76} are not included in this figure as the low-order parameters for these residues amplify the uncertainty in $CSA^{red}/\boldsymbol{S}^2$. The correlation coefficient, *r*, equals 0.50.

As shown in Figure 5, experimentally we observe that a downfield isotropic shift is correlated with an increase in the CSA. Therefore, this means that variations in σ_{11} are larger than those in $(\sigma_{22} + \sigma_{33})/2$. The slope of the correlation observed in Figure 5 is −0.30, which is close to the value of $-^1/_3$, expected if $(\sigma_{22} + \sigma_{33})/2$ were invariant to structural differences. Thus, variations in σ_{22} and σ_{33} must be highly correlated and opposite in sign. This agrees with the remarkable observation by Hiyama et al.[7] for the ^{15}N CSA tensor of a tripeptide where σ_{22} and σ_{33} differ by 47 ppm in the triclinic crystal form, but by only 7 ppm in the monoclinic crystal form, with the isotropic shift and σ_{11} remaining unchanged.

Considering that fluctuations in $(\sigma_{22} + \sigma_{33})/2$ do not contribute significantly to variations in $\sigma_{11} - (\sigma_{22} + \sigma_{33})/2$, the scatter in the correlation shown in Figure 5 must originate from one or more of the following five causes. First, it is possible that all three principal values vary together, i.e., without changing the chemical shift anisotropy. This assumption is implicit when plotting the deviation from random coil chemical shift, $\Delta\delta$, instead of the isotropic shift, δ, itself. ^{15}N chemical shift tensors reported by Oas et al.[6] indicate that the change in isotropic shift between a glycine and a tyrosine residue is approximately the same as the change in the $(\sigma_{22} + \sigma_{33})/2$ values of these two tensors, and therefore provide some justification for using the $\Delta\delta$ instead of δ. Second, there is considerable uncertainty in the random coil ^{15}N shift values, which can differentially affect the $\Delta\delta$ values. For example, the pairwise rmsd between random coil shifts reported by Glushka et al.[37] and Wishart et al.[38] is 2.8 ppm. Third, random error in the measurement of I_A/I_B results in an uncertainty in CSA^{red}, which is further amplified when CSA^{red} is divided by $\boldsymbol{S}^2 \approx 0.85$, and by the uncertainty in $\boldsymbol{S}^2$, estimated at 1%. The random uncertainty in CSA^{red} is estimated by comparing values derived from data measured at $2\Delta = 46.7$ and 68 ms. The pairwise rmsd is 1.4 ppm, indicating a random error of 0.7 ppm in the average, used for deriving the values shown in Figure 5. Thus, the total random error in the $CSA^{red}/\boldsymbol{S}^2$ values is estimated to be *ca.* 1 ppm. Fourth, variations in the angle θ can have a large effect on CSA^{red}.

(37) Glushka, J.; Lee, M.; Coffin, S.; Cowburn, D. *J. Am. Chem. Soc.* **1989**, *111*, 7716−7720.
(38) Wishart, D. S.; Sykes, B. D.; Richards, F. M. *J. Mol. Biol.* **1991**, *222*, 311−333.
(39) Piotto, M.; Saudek, V.; Sklenar, V. *J. Biomol. NMR* **1992**, *2*, 661−665.

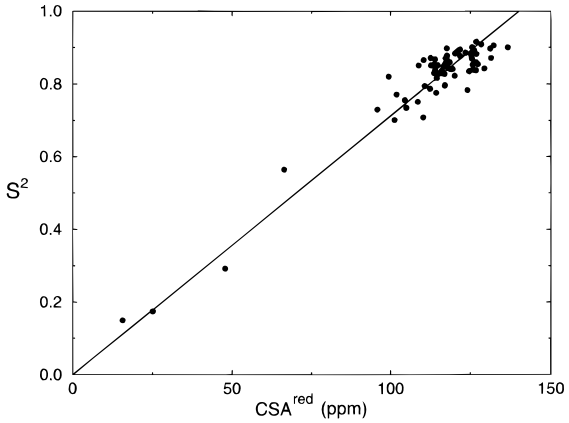

Figure 6. Correlation between the CSA^{red} values in human ubiquitin and the previously measured order parameters.[27] CSA^{red} values are calculated from data recorded at 600 MHz, using $2\Delta = 46.7$ ms, assuming isotropic diffusion with $\tau_c = 4.1$ ns. The solid line corresponds to the correlation expected if $\sigma_{||} - \sigma_{\perp} = -170$ ppm and $\theta = 20°$. The previously measured $\boldsymbol{S}^2$ values deviate from the solid line with a rmsd of 0.045.

Even a small increase in θ from, for example, 20 to 22° decreases the expected $CSA^{red}/\boldsymbol{S}^2$ value by ~6 ppm. It is therefore likely that variations in θ are also a significant source of the scatter observed in Figure 5. Finally, if the orientation of the σ_{11} tensor component is not collinear with the N−H bond vector, the deviation from axial symmetry of the ^{15}N CSA tensor provides an additional contribution to cross correlation and thereby affects the value derived for CSA^{red}. Following Chung et al.,[30] calculations for the case of isotropic tumbling and an asymmetric ^{15}N CSA tensor indicate that the typical values of the ^{15}N CSA asymmetry observed in peptide bond amides affect CSA^{red} by not more than a few percent.

Correlation between CSA^{red} and $\boldsymbol{S}^2$. The magnitude of the relaxation interference effect, η, is directly proportional to the generalized order parameter, $\boldsymbol{S}^2$, and the variability in $\boldsymbol{S}^2$ is considerably larger than the variation in $\sigma_{||} - \sigma_{\perp}$. Therefore, the CSA^{red} values provide information on the relative values of the order parameters of the backbone ^{15}N nuclei. Figure 6 shows the correlation between the order parameters calculated previously from ^{15}N T_1 and T_2 values and the CSA^{red} values calculated using eqs 4 and 8, using an isotropic rotational correlation time of 4.1 ns.[24,27] The solid line corresponds to the relation between CSA^{red} and $\boldsymbol{S}^2$, calculated using $\sigma_{||} - \sigma_{\perp} = -170$ ppm, and $\theta = 20°$. The previously measured order parameters agree to within a root-mean-square deviation (rmsd) of 0.045 with the values calculated from CSA^{red}, assuming a uniform CSA of −170 ppm, $\theta = 20°$, and $\tau_c = 4.1$ ns. The rmsd decreases to 0.040 when the spectral density function appropriate for axially symmetric diffusion (eq 6) and the previously reported principal values of the diffusion tensor are used. As discussed above, this residual rmsd of 0.04 is caused by variations in the magnitude of the CSA and small variations in the angle θ between the dipolar vector and the unique axis of the CSA tensor.

The results shown in Figure 6 indicate that if the rotational correlation time is known, the individual backbone order parameters can be estimated from the CSA^{red} values with an rms uncertainty of less than 0.05. Even if the rotational correlation is not known *a priori*, it is well-established from numerous ^{15}N relaxation studies that the order parameters for most N−H pairs involved in secondary structure cluster are about a value of 0.85. Thus, if I_A/I_B ratios are plotted as a histogram, the most populated I_A/I_B ratio corresponds to an order parameter of ~0.85, and the isotropic rotational correlation time can then be calculated assuming again that $\sigma_{||} - \sigma_{\perp} = -170$ ppm, and $\theta = 20°$. If no clear clustering of the I_A/I_B ratios is observed, this could indicate that the rotational diffusion is substantially anisotropic, or that there is an exceptionally large number of mobile residues in the protein.

Concluding Remarks

We have demonstrated that cross correlation between dipolar and CSA relaxation mechanisms can be quantitatively measured from two simple two-dimensional NMR experiments. For ^{15}N, the experiments offer good sensitivity, approximately a factor of 5 lower than a regular ^{1}H−^{15}N HSQC experiment, and yield information on the magnitude of the chemical shift anisotropy, provided order parameters for the backbone amides have been derived from ^{15}N relaxation measurements.

The average ^{15}N CSA, measured in this manner, is −170 ppm, assuming $\theta = 20°$. This value is about 10 ppm larger than the width of the ^{15}N powder pattern observed in solid-state NMR spectra of small model compounds, but this difference may be caused by the fact that the solid-state NMR powder pattern width is reduced by rapid internal fluctuations of the amide.[7] For example, for an $\boldsymbol{S}^2$ value of 0.9, the width of the powder pattern reduces by 5% relative to the static value. The correlation observed between the CSA and the isotropic shift indicates that the sum of the most shielded CSA tensor components is largely invariant to structural changes.

Provided the rotational correlation time of the protein is known, the measurement of cross correlation yields information on the generalized order parameter $\boldsymbol{S}^2$, i.e., on the amplitude of the rapid internal motions. In contrast to the most commonly used approach, where this number is derived from T_1, T_2, and NOE values, the present method is not affected by line broadening caused by slow conformational exchange. However, as a result of the inherent variations in θ and the magnitude of the ^{15}N chemical shift anisotropy, the precision of the order parameter obtained from the experiments proposed in this paper is limited to *ca.* 5%. The $\boldsymbol{S}^2$ values derived in this manner show improved agreement with order parameters obtained from conventional ^{15}N relaxation measurements when the previously derived axially symmetric diffusion tensor[27] is used instead of isotropic tumbling.

Acknowledgment. We thank Stephan Grzesiek, Dennis Torchia, Rob Tycko, Andy Wang, and Larry Werbelow for useful suggestions and James A. Ferretti (National Heart, Lung and Blood Institute) for use of the AMX-360 spectrometer. This work was supported by the Intramural AIDS Targeted Anti-Viral Program of the Office of the Director of the National Institutes of Health.

Appendix

In the presence of internal motions, there is no rigorous, generally valid relationship between cross- and auto-correlation functions. However, this Appendix shows that if the rotational diffusion of the macromolecule is isotropic and the internal motions can be described as independent, small, equal amplitude, restricted rotations about three mutually orthogonal axes, $\langle P_2(\mu_p(0)\cdot\mu_q(t))\rangle = P_2(\cos(\theta_{pq}))\langle P_2(\mu_i(0)\cdot\mu_i(t))\rangle$, with i = p, q, just as is the case in the absence of internal motions. Moreover, for a more general class of physically plausible small amplitude internal motions, the above is a good approximation if θ_{pq} is sufficiently small.

Unlike auto-correlation functions, cross-correlation functions are not always positive and can even increase with time. Since NMR cross-correlation functions are identical to those that determine the fluorescence depolarization of probes whose

emission and absorption dipoles are not coaxial, they have been extensively studied in the fluorescence literature.[31]

For an isotropically reorienting macromolecule, in the presence of internal motions that are uncorrelated with the overall motion,

$$\langle P_2(\mu_p(0)\cdot\mu_q(t))\rangle = \exp(-t/\tau_c)\,\langle P_2(\mu_p(0)\cdot\mu_q(t))\rangle_{\text{internal}} \equiv \exp(-t/\tau_c)\,C_{pq}(t) \quad \text{(A.1)}$$

In general, $C_{pq}(0) = P_2(\cos\theta_{pq})$. The simplest approximation for $C_{pq}(t)$, which is exact at $t = 0$ and ∞, is

$$C_{pq}(t) = C_{pq}(\infty) + [P_2(\cos\theta_{pq}) - C_{pq}(\infty)]\exp(-t/\tau_e) \quad \text{(A.2)}$$

When p = q, $C_{ii}(\infty)$ is just the square of the generalized order parameter $\boldsymbol{S}_i^2$. In general $\boldsymbol{S}_{dd}^2 \neq \boldsymbol{S}_{cc}^2$ as is commonly assumed, although for ^{15}N in peptide bonds one expects this to be a very good approximation. When p ≠ q, $C_{pq}(\infty) = \int\int d\Omega\, d\Omega' P_2(\mu_p\cdot\mu_q')$ is not necessarily positive and can be greater than $C_{pq}(0)$.

To illustrate the above, consider restricted internal rotations described by the angle γ about the z axis. Then,[31]

$$C_{pq}(t) = \sum_{m=-2}^{2} \langle\exp[im(\gamma(0) - \gamma(t))]\rangle d_{m0}^{(2)}(\theta_p) d_{m0}^{(2)}(\theta_q) \times \cos(m\phi_{pq}) \quad \text{(A.3)}$$

where θ_p and θ_q are the polar angles of μ_p and μ_q, ϕ_{pq} is the difference in their azimuthal angle, and $d_{m0}^{(2)}$ are reduced Wigner rotation matrices. It follows from eq A.3 that

$$C_{pq}(\infty) = \sum_{m=-2}^{2} |\langle\exp(im\gamma)\rangle|^2 d_{m0}^{(2)}(\theta_p) d_{m0}^{(2)}(\theta_q)\cos(m\phi_{pq}) \quad \text{(A.4)}$$

For free rotations, such as apply to methyl groups, $C_{pq}(\infty) = P_2(\cos\theta_p)P_2(\cos\theta_q)$, and $C_{ii}(\infty) = P_2(\cos\theta_i)^2$, i = p, q. For backbone amides the amplitude of rotations is restricted and one has $|\langle\exp(im\gamma)\rangle|^2 \cong 1 - m^2\langle(\delta\gamma)^2\rangle$, where $\langle(\delta\gamma)^2\rangle$ is the mean square of the rotation angle. After some algebra, one finds

$$C_{pq}(\infty) = P_2(\cos\theta_{pq}) - 3\langle(\delta\gamma)^2\rangle \sin\theta_p \sin\theta_q \times (\cos\theta_p\cos\theta_q\cos\phi_{pq} + \sin\theta_p\sin\theta_q\cos 2\phi_{pq}) \quad \text{(A.5)}$$

When p = q, this reduces to

$$C_{qq}(\infty) = 1 - 3\langle(\delta\gamma)^2\rangle\sin^2\theta_q \quad \text{(A.6)}$$

Equation A.5 shows that, depending on geometry, $C_{pq}(\infty)$ can be either smaller or greater than $P_2(\cos\theta_{pq})$.

Equation A.5 can be generalized to include independent, small-amplitude, restricted rotations about one or more additional axes. To lowest order, all one has to do is add analogous terms proportional to $\langle(\delta\gamma_I)^2\rangle$ with coefficients determined by the polar and azimuthal angles with axis I taken as the z axis. To illustrate this, suppose μ_p and μ_q lie in the yz plane, with the z axis bisecting the angle between μ_p and μ_q. If the angle between $\mu_{p,q}$ and the z axis is $\pm\theta/2$, then $P_2(\cos\theta_{pq}) = P_2(\cos\theta)$. Suppose one has independent rotations with mean-square amplitude $\langle(\delta\gamma_I)^2\rangle$, $I = x, y, z$, about the three axes, then

$$C_{pq}(\infty) = P_2(\cos\theta) + 3\langle(\delta\gamma_z)^2\rangle[\sin^2(\theta/2)\cos\theta] - 3\langle(\delta\gamma_y)^2\rangle[\cos^2(\theta/2)\cos\theta] - 3\langle(\delta\gamma_x)^2\rangle[\cos 2\theta] \quad \text{(A.7)}$$

since for rotations about the z axis $\theta_p = \theta_q = \theta/2$ and $\phi_{pq} = \pi$, about the x axis $\theta_p = \theta_q = \pi/2$ and $\phi_{pq} = 2\theta$, and about the y axis $\theta_p = \pi/2 + \theta/2$, $\theta_q = \pi/2 - \theta/2$, and $\phi_{pq} = 0$. Similarly

$$C_{pp}(\infty) = C_{qq}(\infty) = 1 - 3\langle(\delta\gamma_z)^2\rangle\sin^2(\theta/2) - 3\langle(\delta\gamma_x)^2\rangle - 3\langle(\delta\gamma_y)^2\rangle\cos^2(\theta/2) \quad \text{(A.8)}$$

When $\langle(\delta\gamma_z)^2\rangle = \langle(\delta\gamma_x)^2\rangle = \langle(\delta\gamma_y)^2\rangle = \langle(\delta\gamma)^2\rangle$,

$$C_{pq}(\infty) = P_2(\cos\theta)[1 - 6\langle(\delta\gamma)^2\rangle] \quad \text{(A.9)}$$

and

$$C_{qq}(\infty) = 1 - 6\langle(\delta\gamma)^2\rangle \quad \text{(A.10)}$$

It then follows from eq A.2 that

$$C_{pq}(t) = P_2(\cos\theta)C_{qq}(t) \quad \text{(A.11)}$$

as claimed in the beginning of the Appendix. Note, however, that eq A.11 is not exact for arbitrary types of internal motion and applies only to isotropic overall motion. However, provided θ is small, eq A.11 remains a good approximation for other physically reasonable types of internal motion of peptide amides. For example, if $\langle(\delta\gamma_z)^2\rangle = 0$ and $\langle(\delta\gamma_x)^2\rangle = \langle(\delta\gamma_y)^2\rangle = \langle(\delta\gamma)^2\rangle$,

$$C_{pp}(\infty) = C_{qq}(\infty) = 1 - 3\langle(\delta\gamma)^2\rangle[1 + \cos^2(\theta/2)] = 1 - 6\langle(\delta\gamma)^2\rangle(1 - \theta^2/8 + ...) \quad \text{(A.12)}$$

and

$$C_{pq}(\infty) = P_2(\cos\theta)\{1 - 3\langle(\delta\gamma)^2\rangle[\cos^2(\theta/2)\cos\theta + \cos 2\theta]/P_2(\cos\theta)\} = P_2(\cos\theta)\{1 - 6\langle(\delta\gamma)^2\rangle(1 + \theta^2/8 + ...)\} \quad \text{(A.13)}$$

Comparison of eqs A.12 and A.13 confirms that eq A.11 remains a good approximation provided θ is small.

When the rotational diffusion is anisotropic, expressions for the correlation functions become considerably more complex. For example, for axially symmetric rotational diffusion, in the absence of internal motions, one has[30,31]

$$\langle P_2(\mu_p(0)\cdot\mu_q(t))\rangle = \exp(-6D_\perp t)P_2(\cos\theta_p)P_2(\cos\theta_q) + \exp[-(5D_\perp + D_\parallel)t](3/4)\sin(2\theta_p)\sin(2\theta_q)\cos(\phi_{pq}) + \exp[-(2D_\perp + 4D_\parallel)t](3/4)\sin^2(\theta_p)\sin^2(\theta_q)\cos(2\phi_{pq}) \quad \text{(A.14)}$$

where now θ_p and θ_q are the spherical angles describing the orientation of μ_p and μ_q relative to the unique axis of the rotational diffusion tensor. The auto-correlation function is

$$\langle P_2(\mu_i(0)\cdot\mu_i(t))\rangle = \exp(-6D_\perp t)[P_2(\cos\theta_i)]^2 + \exp[-(5D_\perp + D_\parallel)t](3/4)\sin^2(2\theta_i) + \exp[-(2D_\perp + 4D_\parallel)t](3/4)\sin^4(\theta_i) \qquad i = p, q \quad \text{(A.15)}$$

and thus in general $\langle P_2(\mu_p(0)\cdot\mu_p(t))\rangle \neq \langle P_2(\mu_q(0)\cdot\mu_q(t))\rangle \neq \langle P_2(\mu_p(0)\cdot\mu_q(t))\rangle P_2(\cos\theta_{pq})$. Thus, the approach used in the text to treat anisotropic overall motion is far from rigorous, although it is expected to be a reasonable approximation when θ_{pq} is small.

Supporting Information Available: Table with CSA^{red} values, derived from data measured at 360 and 600 MHz ^{1}H frequency for three different durations of the dephasing delay, 2Δ (3 pages). See any current masthead page for ordering and Internet access instructions.

JA960510M